Effect of Zr Doping on the Magnetic and Phase Transition Properties of VO$_2$ Powder

Jing Xu [1,2], Haiying Wang [1,2], Zhihong Lu [3], Zhenhua Zhang [1], Zhaorui Zou [1,2], Ziyang Yu [1], Ming Cheng [1], Yong Liu [1,*] and Rui Xiong [1,*]

[1] School of Physics and Technology and the Key Laboratory of Artificial Micro/Nano Structures of Ministry of Education, Wuhan University, Wuhan 430072, China; xujinghenan@126.com (J.X.); wanghaiy@whu.edu.cn (H.W.); zzhua_mag@whu.edu.cn (Z.Z.); zrzou@whu.edu.cn (Z.Z.); tommyu91@163.com (Z.Y.); chengming-phy@outlook.com (M.C.)
[2] College of Physics and Materials Science, Henan Normal University, Xinxiang 453007, China
[3] School of Materials and Metallurgy, Wuhan University of Science and Technology, Wuhan 430072, China; zludavid@live.com
[*] Correspondence: yongliu@whu.edu.cn (Y.L.); xiongrui@whu.edu.cn (R.X.)

check for updates

Abstract: In this work, V$_{1-x}$Zr$_x$O$_2$ powder (x = 0, 0.01, 0.02, 0.04) was synthesized by two step hydrothermal method. The micro-topography, magnetic and phase transition properties have been investigated using various measurement techniques. All prepared V$_{1-x}$Zr$_x$O$_2$ powder samples exhibit monoclinic structure at room temperature. With the Zr^{4+} ions doping concentration increased, the shapes of VO$_2$ particles change from spherical to rectangular slice. Besides, the saturation magnetic moment of the samples decrease with the increase of doped Zr^{4+} ions concentration, while their phase transition temperature increase gradually with Zr ions doping at a rate of around 2 °C/at% on average. We investigated the Zr doping effects on V-V dimers and confirmed the role of V-V dimers in phase transition. We speculate that more V-V dimers form with Zr doping by magnetic measurements, which result in the monoclinic phase of Zr-doped VO$_2$ sample is more stable than rutile phase. Therefore the phase transition temperature is elevated by Zr doping in our experiment. We further consider that the VO$_2$ phase transition should be ascribed to Peierls transition caused by the changing of V-V dimers.

Keywords: V-V dimer; magnetic properties; phase transition temperature; Zr-doped

1. Introduction

Vanadium dioxide (VO$_2$) is a first-order phase transition material, that transforms itself from a low temperature monoclinic phase [P21/c] to a high temperature rutile phase [P42/mnm] at 68 °C, which resulting in significant changes to its resistance and optical properties [1–3]. Changes to its metal-insulating transition properties can also be triggered by the application of an external electric field or stress [4–6]. Therefore, the unique phase transition properties of VO$_2$ derived materials have been exploited for applications towards smart windows [7], thermoelectric materials [8,9], resistance switch [10–12] and temperature measurement devices [13,14].

However, there are a few problems still limit its practical application, for example, a high phase transition temperature (Tt) of VO$_2$ [15–17]. Ion doping process have been developed to try and address this issue. Doping mainly divided into two types: The first type involves the use of high valence state cations such as W^{6+}, Mo^{5+}, Nb^{5+}, which are known to decrease the phase transition temperature by introducing extra electrons into the VO$_2$ sample [18–20]; The second type is to utilizes low valence state cations, such as Al^{3+}, Cr^{3+}, to increase the phase transition temperature of the VO$_2$ derived

materials [21–23]. However, there is no clear explanation currently existing to clarify the beneficial effects of substitution V^{4+} ions with Ti^{4+} ions or Zr^{4+} ions that have the same valence state. Zhang et al. reported that the phase transition temperature (Tt) rose from 42 °C to 56.7 °C in cooling process; while Tt decreased at Zr/V ratio from 0 to 8.5% and then increased with increase of Zr/V ratio in heating process [24]. Shen et al. reported that Zr doping could decrease the phase transition temperature and improve solar regulation rate simultaneously, the phase transition temperature decreased to 64.3 °C when the zirconium doping concentration was up to 9.8% [25]. Li et al. synthesized VO_2 films with a sol-gel method and found that the effect of Zr^{4+} doping decreased phase transition temperature by approximately 1 °C/at% on average [26]. Lu et al. reported that the phase transition temperature (Tt) decreased with the increase of zirconium doping concentration, the Tt reduced to 50 °C when the zirconium doping concentration up to 2 wt% [27]. Therefore, it is necessary to study the influence of 4-valent ion dopants (Zr^{4+} ions) on the phase transition temperature of VO_2 samples.

In this work, un-doped, 1%, 2% and 4% Zr-doped VO_2 powders were fabricated using a hydrothermal method and their phase transition temperatures, micro-topography and magnetic properties were investigated using different measurement techniques. Experimental results revealed that the phase temperature of these VO_2 samples increased as the amount of Zr doping increased, which may due to Zr mediate the transformation of free V^{4+} ions into V-V dimers that are formed as zigzag chains at low temperature.

2. Experimental Methods

Analytical grade reagents were used for the synthesis without further purification. Highly crystalline $V_{1-x}Zr_xO_2$ (x = 0, 0.01, 0.02, 0.04) samples were synthesized via a two-step hydrothermal method through the reaction of vanadyl acetylacetonate and ethylene glycol, with zirconium nitrate pentahydrate used as a doping source. 0.4 g of vanadyl acetylacetonate and a specified molar ratio of zirconium nitrate pentahydrate were dissolved in an aqueous solution of glycol. This mixed solution was then heated in a 100 mL autoclave at 200 °C for 24 h to obtain a powder which was washed several times and then dried at 60 °C in a drying oven. The resultant powder was then annealed under a high-purity Ar atmosphere at 500 °C for 15 h to obtain highly crystalline un-doped VO_2 powder, 1% Zr-doped VO_2 powder, 2% Zr-doped VO_2 powder and 4% Zr-doped VO_2 powder.

The structure of the VO_2 powder samples were characterized by X-ray diffraction (XRD, D8 Brucker, Karlsruhe, Germany). The surface micro-topography of the samples were observed using field emission scanning electron microscope (FE-SEM, Zeiss SIGMA, Carl Zeiss Microscopy Ltd., Cambridge CB1 3JS, UK) and their phase transition temperatures obtained from their thermal hysteresis loops. The elemental compositions of the samples were determined by X-ray photoelectron spectroscopy (XPS, ESCALAB 250Xi, Thermo Fisher Scientific, Waltham, MA, USA) and the magnetic properties were analyzed using a vibrating sample magnetometer (VSM, Quantum Design PPMS, San Diego, CA, USA) using a magnetic field of 10 K Oe.

3. Results and Discussion

The crystal phase structures of samples un-doped, 1% Zr-doped, 2% Zr-doped VO_2 and 4% Zr-doped VO_2 powder were determined from their XRD patterns measured for a 2θ range from 20° to 80° shown in Figure 1a, which revealed that all the samples have monoclinic structure (space group P21/c, standard lattice parameters form PDF card: a = 0.575 nm, b = 0.454 nm, c = 0.538 nm and β = 122.64°, JCPDS No. 43-1051). No oxides of Zr were detected in the diffraction patterns, eVen when the Zr content was as high as 4%, which indicates that the Zr had been effectively doped into the VO_2 lattice. Figure 1b shows a magnified view of the XRD peak corresponding to the (011) lattice plane. The peak shifted slightly towards the small angle, indicating that Zr doping had resulted in an expanded lattice [26,27]. The reason is that the doped Zr^{4+} ions have a higher radius (0.072 nm) than the V^{4+} ions (0.058 nm). The grain size of the samples decreased gradually with the increased of Zr

doping concentration, which indicates that Zr doping increases the number of defect sites to promote the formation of multiple nucleation centers [28].

The interplanar spacing values were calculated using the formula $2d\sin\theta = \gamma$, where θ is the Bragg's diffraction angle and γ is the wavelength of the X-ray which equals to 0.154 nm (Cu Kα radiation). The grain sizes of the selected lattice plane were calculated using the Debye-Scherrer's equation: $D = K\gamma/B\cos\theta$, where K is the Scherrer's constant which equals to 0.89, γ is the wavelength of X-ray, B is the full width at half-maximum (FWHM) (in rad) and θ is the Bragg's diffraction angle (in degrees). The unit cell volume for monoclinic VO_2 was calculated using $V = a*b*c*\sin\beta$, where a, b and c are lattice constants and β is the angle of b-axis with the AOC plane. The lattice parameters and the volume of the unit cells of un-doped, 1% Zr-doped, 2% Zr-doped and 4% Zr-doped VO_2 samples are showed in Table 1. The calculated results of the lattice volumes increased gradually with the increase of Zr doping concentration, because the doped Zr^{4+} ions have a larger ionic radius than that of V^{4+} ions.
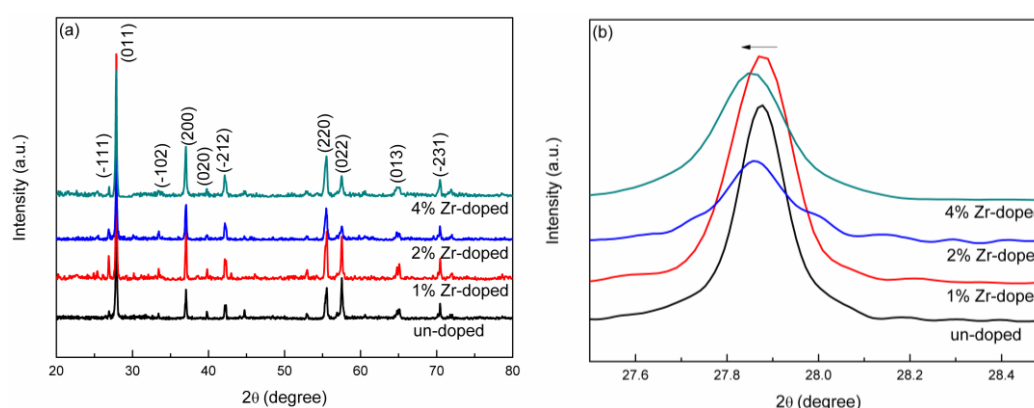

Figure 1. (**a**) X-ray diffraction (XRD) patterns and (**b**) Enlarged X-axis patterns from 27.5° to 28.5° of un-doped, 1% Zr-doped, 2% Zr-doped and 4% Zr-doped VO_2 samples.

Table 1. Grain size, d_{011} interplanar spacing, lattice parameters and volume of the unit cells of un-doped, 1% Zr-doped, 2% Zr-doped and 4% Zr-doped VO_2 samples.

Sample	2θ-d_{011} (°)	d_{011} (nm)	Grain Size (nm)	a (Å)	b (Å)	c (Å)	β (°)	V = abcsin β (Å³)
un-doped	27.910°	3.1940	50.6	5.7435	4.5200	5.3472	122.4186	117.1826
1% Zr-doped	27.890°	3.1963	49.07	5.7604	4.5226	5.3658	122.6497	117.7008
2% Zr-doped	27.877°	3.1977	38.92	5.7578	4.5298	5.3615	122.6428	117.7497
4% Zr-doped	27.868°	3.1988	38.73	5.7607	4.5288	5.3659	122.6391	117.8845

The effect of Zr doping on the morphology of VO_2 samples was measured using FE-SEM analysis (Figure 2a–d). The un-doped VO_2 samples are nano-sphere with some of them aggregate together (Figure 2a), while Zr doped VO_2 samples exhibit both spherical and rod-like particles (Figure 2b,c). With the concentration of Zr dopant increased, some of the rod-like particles were found to combine to form extended slices. For example, the SEM images of 4% Zr-doped VO_2 samples shown in Figure 2d reveal that the majority of VO_2 particles combined into a sheet-like form, with only a few remaining in their granular ball shape. Due to the large differences of electron-negativity between V (1.63) element and Zr (1.33) element, the bond energy of Zr-O bond is larger than that of V-O band. The V-O bond was replaced by Zr-O band and the Gibbs free energy per unit volume of the system goes down with Zr^{4+} ions doping into VO_2 lattice. And the critical nucleation energy decreases, simultaneously, which leads to the higher density of crystal nucleus. In a word, the doping of Zr ions increase the number of defect-nucleation sites [28] and serve to prevent the growth of VO_2 in specific directions. The grain size of un-doped, 1% Zr-doped, 2% Zr-doped and 4% Zr-doped VO_2 samples decreasing gradually, while grain density increase gradually with the increase of Zr doping concentration.
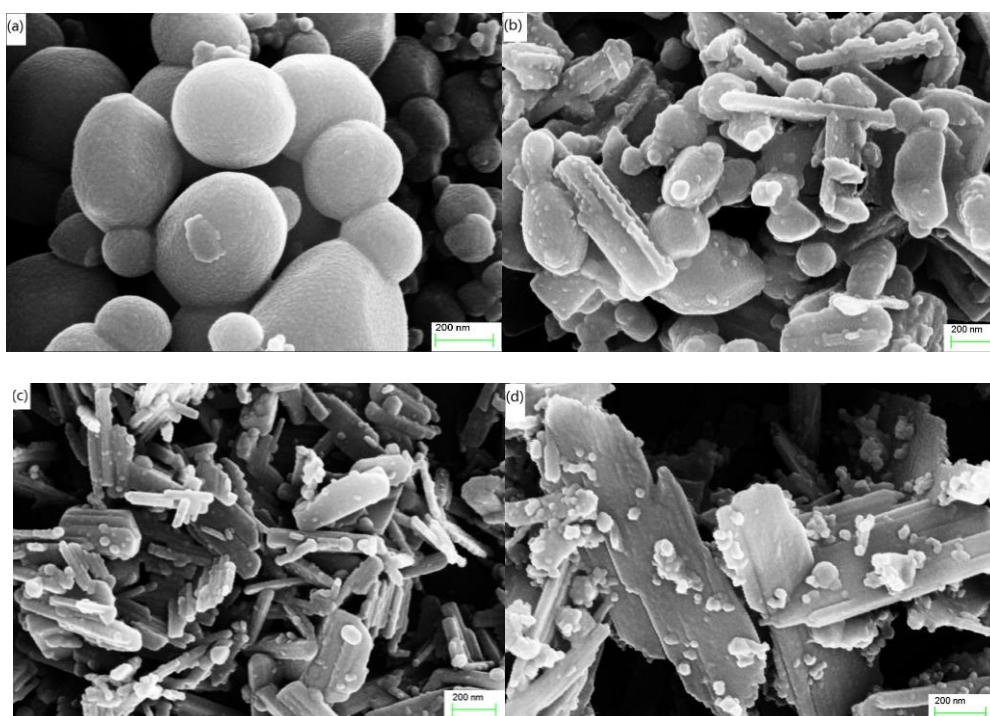
Figure 2. (**a**–**d**) FE-SEM (field emission scanning electron microscope) micro-topographic images of the un-doped, 1% Zr-doped, 2% Zr-doped and 4% Zr-doped VO_2 samples, respectively. All images were observed in InLens mode with an accelerated voltage of 15 kV.

The element chemical states of the samples were investigated using XPS analysis, with XPS spectra for Zr, V and O element. Figure 3a shows the full range spectra of the un-doped and 4% Zr-doped samples, binding energy (BE) ranging from 0 to 1200 eV. Two weak peaks appeared at BE around 190 eV and 320 eV were marked with cyan square in the 4% Zr-doped samples corresponding to Zr 3d and 3p energy levels [29], respectively. This demonstrates the Zr ions successfully doped into the VO_2 lattice. Due to the BE of V 2p and O 1s is approaching, their core level spectra are shown together in Figure 3b. The peaks at BE of 517.53 eV and 524.74 eV correspond to V^{4+} valences, V $2p_{3/2}$ and $2p_{1/2}$ states, respectively [18]. And the distance between doublets was 7.2 eV consistent with Zou et al. report [18]. A weak O 1s peak at 520.96 eV corresponding to O 1s X-ray satellite peak was also present [30]. A main peak appeared at 530.59 eV corresponding to a typical lattice O^{2-} absorption that has been reported for many metal oxides (e.g. TiO_2 and VO_2) [31,32]. A peak appeared with a BE of 532.56 eV was assigned to C=O and hydroxyl groups that probably result from contamination of sample [31]. In Figure 3c, two peaks appeared at BE of 182.31 eV and 184.75 eV which correspond to Zr $2p_{3/2}$ and $2p_{1/2}$ energy levels, respectively [33] Thus confirming that Zr^{4+} had been effectively doped into the VO_2 lattice.

The magnetic moment versus temperature curves of the samples reveal abrupt increases in their magnetic moments for increasing temperature in Figure 4. (Moment vs applied field curves of un-doped VO_2 powder samples before and after phase transition (300K and 350K are showed in Figure S1). The rutile phase of un-doped VO_2 samples have the largest magnetic moment of 0.07 emu/g, while the 4% Zr-doped samples have the lowest magnetic moment of 0.039 emu/g. For VO_2 rutile phase, it is known that V^{4+} ions are periodically arranged in straight chains, with eVery V^{4+} ion having a free electron that contributes a magnetic moment of s = 1/2 [34]. The magnetic moment of the rutile phase arises from the presence of free V^{4+} ions and the doped Zr^{4+} ions contribute approximately zero to the overall magnetic moment. Therefore, the doping of Zr^{4+} ions leads to an overall decrease in the saturation magnetic moment of the VO_2 derived material.
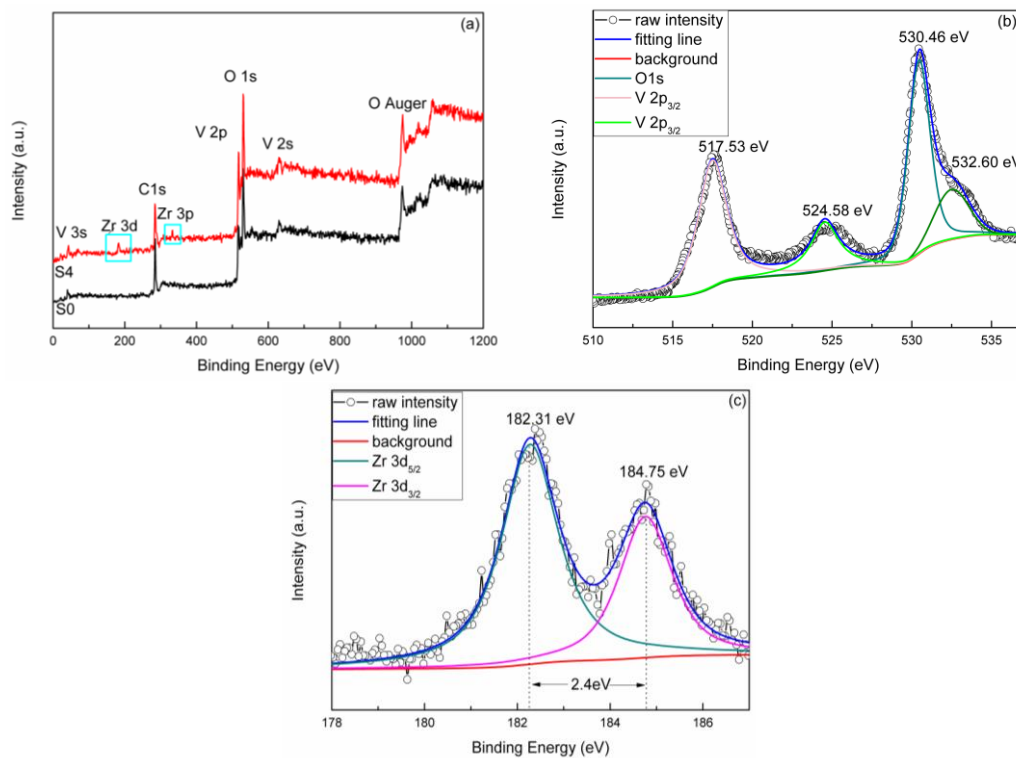
Figure 3. (**a**) XPS (X-ray photoelectron spectroscopy) spectra of un-doped and 4% Zr-doped VO_2 samples with binding energy from 0 to 1200 eV; (**b**) Core level for V 2p and O 1s of 4% Zr-doped VO_2 samples; (**c**) Core level for Zr 3d of 4% Zr-doped VO_2 samples.
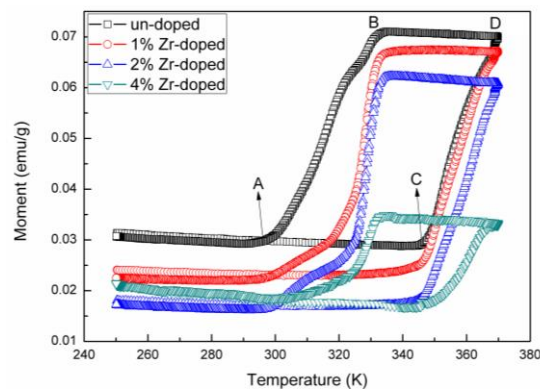

Figure 4. Moment vs. Temperature curves of un-doped, 1% Zr-doped, 2% Zr-doped and 4% Zr-doped VO_2 samples from 250 K to 370 K in a 10 k Oe magnetic field.

For VO_2 monoclinic phase, the main difference with the VO_2 rutile phase is the formation of V-V dimers [35]. The paired V-V dimers that are formed as zigzag chains arranged in an approaching antiparallel direction, approximately contributing a zero magnetic moment. Besides the paired V-V dimers, some unpaired free V^{4+} ions may also be present in the monoclinic [36]. For Zr doped VO_2 samples, the total magnetic moment is given by $M_{total} = M_{dimers} + M_{free} + M_{Zr}$. Therefore, when Zr is doped into the VO_2 lattice, the magnetic moment decreased significantly, which means that it not only related to the substitution of V^{4+} ions but also the formation of V-V dimers. It is proposed that Zr^{4+} act as initiators to promote conversion of free V^{4+} ions into zigzag V-V dimer that results in an overall decrease in the total magnetic moment. The mechanism of Zr^{4+} ion dopants which promotes dimer formation is unknown, however it is clear that free V^{4+} ions in the high temperature state have a much larger magnetic moment than V-V dimers in the low temperature state.

The phase transition temperatures of the doped materials were obtained from their thermal hysteresis loops (The first-order transition was proved in Figure S2). Therefore, thermal hysteresis loops for each sample were calculated using the equation $T_{cool} = [T_A + T_B]/2$, $T_{heat} = [T_C + T_D]/2$ and $T = [T_{cool} + T_{heat}]/2$, where A, B, C and D are the corresponding magnetic moment inflection points. From Table 2, it can be seen that T_{heat}, T_{cool} (T_{heat} and T_{cool} are the phase transition temperatures in heating and cooling process, respectively) and the Tt of the material increased with Zr doping concentration increased. The T_{heat} increased slowly (0.5 K /at% doped Zr ions) with Zr doping levels increased compared with the changes of T_{cool} (4 K/at% doped Zr ions). The Zr-doped VO_2 films prepared by Zhang et al. had the same tendency in cooling process [24]. However, Shen et al., Li et al. and Lu et al. have the opposite results with our experiment results [25–27]. They attributed the decreased of Tt to the changes of lattice structure. But in our experiment, except for changes of the lattice structure, the magnetic properties have a big difference after Zr doping into VO_2 lattice, which means a mechanism associated with V-V dimers accounted for the elevated phase transition temperature.

Table 2. Cooled (T_{cool}), heated (T_{heat}) and mean phase transition temperatures (T) calculated from moment vs. temperature curves of un-doped, 1% Zr-doped, 2% Zr-doped and 4% Zr-doped VO_2 samples.

Sample	T_{cool} (K)	T_{heat} (K)	$T = [T_{cool} + T_{heat}]/2$ (K)
un-doped	315.06	357.08	336.07
1% Zr-doped	327.29	357.8	342.55
2% Zr-doped	327.8	358.8	343.30
4% Zr-doped	328.22	359.3	343.76

The charge doping effect of high valence state ions normally results in materials with lower phase transition temperatures, while low valence state ions are known to increase their phase transition temperatures. This means that Zr^{4+} ions dopants do not modify the phase transition properties of VO_2 systems through a charge doping effect. Therefore, the observed changes in the phase transition temperature are likely to be caused through a mechanism that rely on Peierls type electron phonon correlations [37–39]. Tomczak et al. have previously applied a lattice "Peierls substitution" method to calculate the optical conductivities of metallic and insulating states of multi-atomic unit cells and their calculated results found to be in good agreement with experimental results [37]. Kim et al. also reported that the phase transition mechanism of VO_2 could be modelled effectively using an orbital-selective Peierls transition method that employed DFT+U calculations [38]. For VO_2, the outermost electronic configuration of V^{4+} ion is d^1, which means that each ion has one conducting electron. Its Fermi energy level appears at 1/2 position of the energy band, with the half empty energy states and the half occupied energy states. When V-V dimers are formed then the lattice is distorted, with the lattice constant for the quasi-1D V chains effectively doubled to produce a Fermi level with an increased energy gap that results in the decreasing of overall energy of the system. The boundary of the Brillouin zone of these distorted lattice corresponds to the Fermi level, which can change from a high energy metal state to a low energy insulated state. Then, Peierls phase transition occurred due to the fluctuation of charge density wave. Besides, S. Biermann et al. reported that VO_2 is not a conventional Mott insulator and formation of V-V dimers plays an important role in triggering the creation of Peierls gaps in the insulted material [39]. Doping Zr into the VO_2 system perhaps results in an overall increase in the number of V-V dimers present, with the V-V dimers of Zr requiring more energy to dissolve to enable the material to complete phase transition. We speculate that more V-V dimers are formed with Zr doping, which result in the low temperature state is more stable than high temperature state. Therefore the phase transition temperature is elevated by Zr doping in our experiment. Besides, it has previously been reported that cationic dopants with empty d orbitals are more stable in low anion coordination states, therefore Zr^{4+} is acting to stabilize the low monoclinic phase of VO_2 [40], which

results in more energy being required to complete the phase transition process. The increased number of V-V dimers has a bigger influence than lattice changes on Zr doping VO$_2$ samples.

4. Conclusions

The un-doped, 1%, 2% and 4% Zr-doped VO$_2$ powder were prepared using a hydrothermal method. It was found that Zr and V existed in the forms of Zr^{4+} and V^{4+} states, respectively. No XPS peaks corresponding to V^{3+} and V^{5+} were present in all the samples. Doping of Zr ions change the shape of the spherical un-doped VO$_2$ particles into the doped VO$_2$ rectangular slice shape. The saturation magnetic moments of the samples increased gradually with the increase of Zr doping concentration. The phase transition temperatures of Zr-doped VO$_2$ samples were elevated from 336.07 K to 343.76 K, which were correlated to Zr ion doping concentration. We speculate that more V-V dimers are formed with Zr doping by magnetic measurements, which results in the monoclinic phase of Zr-doped VO$_2$ sample is more stable than rutile phase. Therefore the phase transition temperature is elevated by Zr doping in our experiment. And the VO$_2$ phase transition should be ascribed to Perils transition caused by changing of V-V dimers.

References

1. Morin, F.J. Oxides which show a metal-to -insulator transition at the Neel temperature. *Phys. Rev. Lett.* **1959**, *3*, 34–36. [CrossRef]
2. Kang, L.; Gao, Y.; Luo, H.; Chen, Z.; Du, J.; Zhang, Z. Nanoporous thermochromic VO$_2$ films with low optical constants, enhanced luminous transmittance and thermochromic properties. *ACS Appl. Mater. Interfaces* **2011**, *3*, 135–138. [CrossRef]
3. Babulanam, S.M.; Eriksson, T.S.; Niklasson, G.A.; Granqvist, C.G. T hermochromic VO$_2$ films for energy-efficient windows. *Solar Energy Mater.* **1987**, *6*, 347–363. [CrossRef]
4. Wu, B.; Zimmers, A.; Aubin, H.; Ghosh, R.; Liu, Y.; Lopez, R. Electric-field-driven phase transition in vanadium dioxide. *Phys. Rev. B* **2011**, *84*, 241410. [CrossRef]
5. Chen, Y.; Wang, Z.; Chen, S.; Ren, H.; Li, B.; Yan, W.; Zhang, G.; Jiang, J.; Zou, C. Electric-field control of Li-doping induced phase transition in VO$_2$ film with crystal facet-dependence. *Nano Energy* **2018**, *51*, 300–307. [CrossRef]
6. Sohn, J.I.; Joo, H.J.; Kim, K.S.; Yang, H.W.; Jang, A.R.; Ahn, D.; Lee, H.H.; Cha, S.N.; Kang, D.J.; Kim, J.M. Stress-induced domain dynamics and phase transitions in epitaxially grown VO$_2$ nanowires. *Nanotechnology* **2012**, *23*, 205707. [CrossRef] [PubMed]
7. Dai, L.; Chen, S.; Liu, J.; Gao, Y.; Zhou, J.; Chen, Z.; Cao, C.; Luo, H.; Kanehira, M. F-doped VO$_2$ nanoparticles for thermochromic energy-saving foils with modified color and enhanced solar-heat shielding ability. *Phys. Chem. Chem. Chem.* **2013**, *5*, 11723–11729. [CrossRef]
8. Wu, C.; Feng, F.; Feng, J.; Dai, J.; Peng, L.; Zhao, J.; Yang, J.; Si, C.; Wu, Z.; Xie, Y. Hydrogen-incorporation stabilization of metallic VO$_2$ (R) phase to room temperature, displaying promising low-temperature thermoelectric effect. *J. Am. Chem. Soc.* **2011**, *133*, 13798–13801. [CrossRef]

9. Khan, G.R.; Kandasami, A.; Bhat, B.A. Augmentation of thermoelectric performance of VO_2 thin films irradiated by 200 MeV Ag^{9+}-ions. *Radiat. Phys. Chem.* **2016**, *123*, 55–62. [CrossRef]

10. Kim, J.; Ko, C.; Frenzel, A.; Ramanathan, S.; Hoffman, J.E. Nanoscale imaging and control of resistance switching in at room temperature. *Appl. Phys. Lett.* **2010**, *96*, 213106. [CrossRef]

11. Rupp, J.A.J.; Querre, M.; Kindsmuller, A.; Besland, M.P.; Janod, E.; Dittmann, R.; Waser, R.; Wouters, D.J. Different threshold and bipolar resistive switching mechanisms in reactively sputtered amorphous undoped and Cr-doped vanadium oxide thin films. *J. Appl. Phys.* **2018**, *123*, 044502. [CrossRef]

12. Chen, C.; Lin, C.; Chen, P.; Chang, T.; Shih, C.; Tseng, Y.; Zheng, H.; Chen, Y.; Chang, Y.; Lin, C.; et al. The demonstration of increased selectivity during experimental measurement in filament-type vanadium oxide-based selector. *IEEE Trans. Electron. Devices* **2018**, *65*, 4622–4627. [CrossRef]

13. Guo, H.; Khan, M.I.; Cheng, C.; Fan, W.; Dames, C.; Wu, J.; Minor, A.M. Vanadium dioxide nanowire-based microthermometer for quantitative eValuation of electron beam heating. *Nat. Commun.* **2015**, *5*, 1–5. [CrossRef] [PubMed]

14. Shi, R.; Wang, J.; Cai, X.; Zhang, L.; Chen, P.; Liu, S.; Zhang, L.; Ouyang, W.; Wang, N.; Cheng, C. Axial modulation of metal-insulator phase transition of VO_2 nanowires by graded doping engineering for optically readable thermometers. *J. Phys. Chem. C* **2017**, *121*, 24877–24885. [CrossRef]

15. Zhang, J.; He, H.; Yie, Y.; Pan, B. Giant reduction of the phase transition temperature for beryllium doped VO_2. *Phys. Chem. Chem. Phys.* **2013**, *15*, 4687–4690. [CrossRef]

16. Liu, X.; Wang, S.; Chen, F.; Yu, L.; Chen, X. Tuning phase transition temperature of VO_2 thin films by annealing atmosphere. *J. Phys. D. Appl. Phys.* **2015**, *48*, 265104. [CrossRef]

17. Li, S.Y.; Niklasson, G.A.; Granqvist, C.G. Thermochromic fenestration with VO_2-based materials: Three challenges and how they can be met. *Thin Solid Films* **2012**, *520*, 3823–3828. [CrossRef]

18. Zou, J.; Shi, H.; Su, X.; Feng, Q.; Liang, S. A simple method to prepare $V_{1-x}W_xO_2$ (x = 0, 0.01, 0.02, 0.03, 0.04, and 0.05) controllable phase transition temperature powder. *J. Alloy. Compd.* **2017**, *708*, 706–712. [CrossRef]

19. Khan, G.R.; Asokan, K. Ahmad, Bilal, Room temperature tunability of Mo-doped VO_2 nanofilms across semiconductor to metal phase transition. *Thin Solid Films* **2017**, *625*, 155–162. [CrossRef]

20. Wang, Z.; Zhang, R.; Chen, X.; Fu, Q.; Li, C.; Yuan, S.; Zhao, X.; Tao, H. Nb doping effect in VO_2 studied by investigations of magnetic behavior. *Ceram. Int.* **2018**, *44*, 8623–8627. [CrossRef]

21. Tan, X.; Liu, W.; Long, R.; Zhang, X.; Yao, T.; Liu, Q.; Sun, Z.; Cao, Y.; Wei, S. Symmetry-controlled structural phase transition temperature in chromium-doped vanadium dioxide. *J. Phys. Chem. C* **2016**, *120*, 28163–28168. [CrossRef]

22. Yanase, I.; Mori, Y.; Kobayashi, H. Hydrothermal synthesis and thermal change in IR reflectance of Al/W co-doped VO_2 powder. *Mater. Res. Bull.* **2018**, *100*, 243–248. [CrossRef]

23. Niu, C. Al-doped VO_2 (B) nanobelts as cathode material with enhanced electrochemical properties for lithium-ion batteries. *Funct. Mater. Lett.* **2018**, *11*, 1850068. [CrossRef]

24. Zhang, H.; Wu, Z.; Wu, X.; Wei, X.; Jiang, Y. Preparation and phase transition Properties of nanostructured zirconium-doped vanadium oxide films by reactive magnetron sputtering. *Thin Solid Films* **2014**, *568*, 63–69. [CrossRef]

25. Shen, N.; Chen, S.; Chen, Z.; Liu, X.; Cao, C.; Dong, B.; Luo, H.; Liu, J.; Gao, Y. The synthesis and performance of Zr-doped and W–Zr-codoped VO_2 nanoparticles and derived flexible foils. *J. Mater. Chem. A* **2014**, *2*, 15087. [CrossRef]

26. Li, Y.; Liu, J.; Wang, D.; Dang, Y. Effects of zirconium ions doping on the structural and thermochromic properties of VO_2 thin films. *J. Electron. Mater.* **2017**, *46*, 6466–6472. [CrossRef]

27. Lu, W.; Zhao, G.; Song, B.; Li, J.; Zhang, X.; Han, G. Preparation and thermochromic properties of sol-gel-derived Zr-doped VO_2 films. *Surf. Coat. Tech.* **2017**, *320*, 311–314. [CrossRef]

28. Hu, Y.; Shi, Q.; Huang, W.; Zhu, H.; Yue, F.; Xiao, Y.; Liang, S.; Lu, T. Preparation and phase transition properties of Ti-doped VO_2 films by sol-gel process. *J. Sol-Gel Sci. Technol.* **2016**, *78*, 19–25. [CrossRef]

29. Wagner, C.D.; Riggs, W.M.; Davis, L.E.; Moulder, J.F.; Muilenberg, G.E. Standard ESCA spectra of the elements and line energy information. In *Handbook of X-ray Photoelectron Spectroscop*; Muilenberg, G.E., Ed.; Perkin-Eimer Corporation: Eden Prairie, MN, USA, 1979; Chapter II; p. 101.

30. Wagner, C.D.; Riggs, W.M.; Davis, L.E.; Moulder, J.F.; Muilenberg, G.E. Standard ESCA spectra of the elements and line energy information. In *Handbook of X-ray Photoelectron Spectroscopy*; Muilenberg, G.E., Ed.; Perkin-Eimer Corporation: Eden Prairie, MN, USA, 1979; Chapter II; p. 70.

31. Xu, J.; Wang, H.; Zhou, Z.; Zou, Z. Ferromagnetic properties of N-doped and undoped TiO_2 rutile single-crystal wafers with addition of tungsten trioxide. *Materials* **2018**, *11*, 1934. [CrossRef]

32. Zhang, H.; Yu, H.; Chen, Z.; Luo, H.; Gao, Y. Thermal kinetic analysis of metal -insulator transition mechanism in W-doped VO_2. *J. Therm. Anal. Calorim.* **2016**, *126*, 949–957. [CrossRef]

33. Wagner, C.D.; Riggs, W.M.; Davis, L.E.; Moulder, J.F.; Muilenberg, G.E. Standard ESCA spectra of the elements and line energy information. In *Handbook of X-ray Photoelectron Spectroscopy*; Muilenberg, G.E., Ed.; Perkin-Eimer Corporation: Eden Prairie, MN, USA, 1979; Chapter II; p. 100.

34. Zhang, R.; Yin, C.; Fu, Q.; Li, C.; Qian, G.; Chen, X.; Lu, C.; Yuan, S.; Zhao, X.; Tao, H. Metal-to-insulator transition and its effective manipulation studied from investigations in $V_{1-x}Nb_xO_2$ bulks. *Ceram. Int.* **2018**, *44*, 2809–2813. [CrossRef]

35. Park, J.H.; Coy, J.M.; Kasirga, T.S.; Huang, C.; Fei, Z.; Hunter, S.; Cobden, D.H. Measurement of a solid-state triple point at the metal–insulator transition in VO_2. *Nature* **2013**, *500*, 431–434. [CrossRef] [PubMed]

36. Yin, C.; Zhang, R.; Qian, G.; Fu, Q.; Li, C.; Wang, M.; Zhu, C.; Wang, L.; Yuan, S.; Zhao, X.; et al. Unusual magnetic transition near metal-insulator transition and paramagnetic anomaly in VO_2. *Appl. Phys. Lett.* **2017**, *110*, 172404. [CrossRef]

37. Tomczak, J.M.; Biermann, S. Optical properties of correlated materials: Generalized Peierls approach and its application to VO_2. *Phys. Rev. B* **2009**, *80*, 085117. [CrossRef]

38. Kim, S.; Kim, K.; Kang, C.J.; Bin, B.I. Correlation-assisted phonon softening and the orbital-selective Peierls transition in VO_2. *Phys. Rev. B* **2013**, *87*, 195106. [CrossRef]

39. Biermann, S.; Poteryaev, A.; Lichtenstein, A.I.; Georges, A. Dynamical Singlets and Correlation-Assisted Peierls Transition in VO_2. *Phys. Rev. Lett.* **2005**, *94*, 026404. [CrossRef] [PubMed]

40. Krammer, A.; Magrez, A.; Vitale, W.A.; Mocny, P.; Jeanneret, P.; Guibert, E.; Whitlow, H.J.; Ionescu, A.M.; Schuler, A. Elevated transition temperature in Ge doped VO_2 thin film. *J. Appl. Phys.* **2017**, *122*, 045304. [CrossRef]